

Wafer scale Ge-on-Si metalens for the mid-infrared

Yanyan Zhou¹, Qize Zhong¹, Zhihao Ren², Landobasa Y. M. Tobing¹, Yuan Hsing Fu¹, Rachel Ang¹, Bo Li¹, Hong Zhou², Chengkuo Lee², Lennon Y. T. Lee^{*1}

¹Institute of Microelectronics, Agency for Science Technology and Research, 2 Fusionopolis Way, #08-02, Innovis, Singapore 138634

²Department of Electrical and Computer Engineering, National University of Singapore, 4 Engineering Drive 3, Singapore 117576

*Corresponding author: Lennon-lee@ime.a-star.edu.sg

Abstract: We report the first demonstration of metalens devices fabricated on an 8-inch Ge-on-Si wafer for the mid-infrared regime. Experimental observations of beam focusing show good match with the design.

OCIS codes: (220.0220) Optical design and fabrication; (110.5220) Photolithography; (310.6628) Subwavelength structures, nanostructures.

1. Introduction

Mid-infrared (mid-IR) is a technologically important band and is crucial to many applications including thermal imaging, remote sensing and free-space communications. However, most of the mature materials are opaque in this range, making the development of mid-IR photonics challenging. Up till now, the majority of meta-structures working in the mid-IR are realized by metals which often limit the device operation to the reflection mode [1-2]. Huygens metasurface was realized through a chalcogenide alloy platform while demonstrating good device performances [3]. Unfortunately, chalcogenide is not complementary metal-oxide-semiconductor (CMOS) compatible. In Ref. [4], wafer scale fabrication of mid-IR metasurfaces was demonstrated with freestanding Ge meta-structures on Al₂O₃ membrane. Although a CMOS-compatible platform, structural fragility of the membrane precludes the realization of large area devices and mechanical robustness. Moreover, the fabrication processes are complicated due to the membrane formation.

In this work, we report the first demonstration of metalenses fabricated from 8-inch Ge-on-Si wafers. The devices are fabricated using standard 8-inch CMOS-compatible fabrication line and subsequently characterized by a laser-based IR microscope (Spero QT).

2. Device Design, Fabrication and Characterization

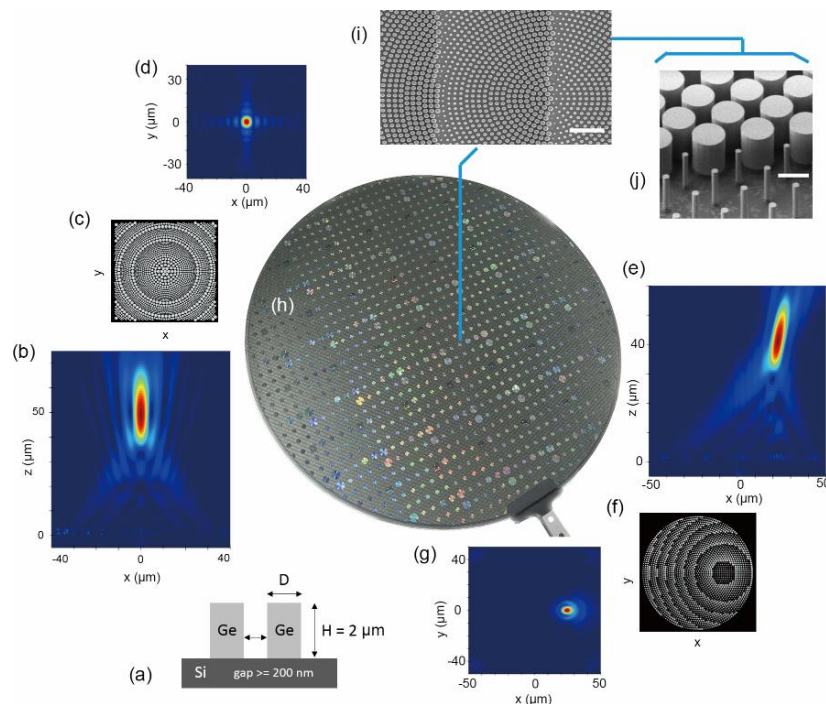


Fig. 1 (a) Schematic showing side view of Ge pillars on Si substrate; (b) E-field distribution in the propagation (xz) plane (c) top view of structures (d) E field distribution in the focal (xy) plane for the simulated on-axis focusing metalens (aperture $AP = 80 \mu\text{m}$, $f = 50 \mu\text{m}$); (e) E-field distribution in xz -plane (f) top view of structures (g) E-field distribution in the xy -plane for the simulated off-axis focusing metalens ($AP = 100 \mu\text{m}$, $f = 40 \mu\text{m}$); (h) photograph of fabricated Ge-on-Si metasurfaces on an 8-inch wafer; SEM images of (i) top view (j) side view of part of the metalens indicated in (h).

As shown by the side view schematic of Fig. 1(a), the designed metalens is consisted of Ge pillars standing on a Si substrate. While the height of the pillars is $2 \mu\text{m}$ throughout, the diameters vary from 0.2 to $1.6 \mu\text{m}$, with the smallest inter-pillar gap as 200 nm . The same finite-difference time-domain (FDTD) simulation model used in Ref. [5] is adopted here to study two types of devices – the on-axis and the off-axis focusing lenses. The metalens rests in the xy -plane at $z = 0$; incident plane wave from $-z$ passes through the metalens and focuses at $z = f$ (focal length). Figure 1(b) and (d) shows E-field intensity distribution in the propagation (xz) and focal (xy) plane respectively. Beam focusing in the center of the xy -plane [Fig.1(d)] indicates on-axis focusing. In contrast, as displayed by Fig. 1(e) and (g), the off-axis focusing results in oblique propagation for the focused beam, i.e. the beam is off-center.

The fabrication processes of the metalens devices are straightforward and CMOS-compatible. Single crystalline Ge thin film with thickness of $2 \mu\text{m}$ is first grown on an 8-inch Si wafer using chemical vapor deposition. We then use 193nm ArF DUV scanner and deep reactive-ion etching (DRIE) to make the Ge pillars of the metasurfaces. Figure 1(h) shows the photograph of fabricated Ge-on-Si metalenses on an 8-inch wafer. The SEM image in Fig. 1(i) reveals the top view of part of an off-axis metalens (scale bar is $10 \mu\text{m}$), while Fig. 1(j) shows the side view of a series of pillars with different diameters (scale bar is $2 \mu\text{m}$). Good uniformity is achieved for the wafer-scale metasurface fabrication and an average sidewall angle of 89.5° is observed for pillars of all sizes.

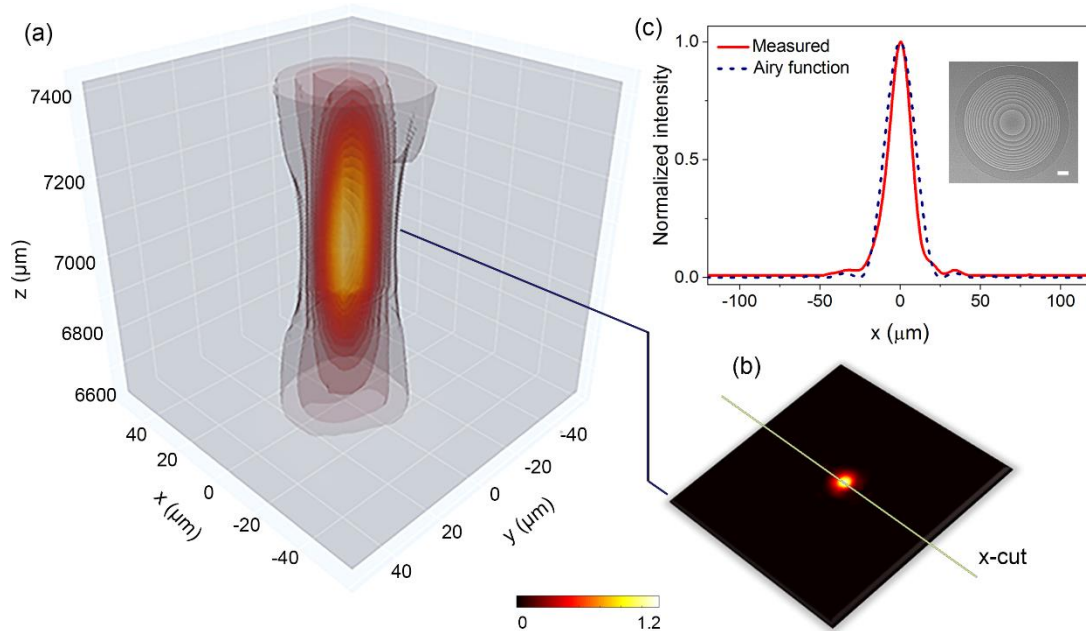


Fig. 2 Measurement data for the on-axis focusing metalens: (a) 3-D intensity profile around the focal point; (b) xy intensity profile at $z = 7.05 \text{ mm}$; (c) x -cut intensity plot of (b) at $y = 0$ with the Airy function drawn as reference, inset: SEM image of the full on-axis focusing metalens (scale bar = $200 \mu\text{m}$).

Performance of the fabricated metalenses is measured using the Spero QT hyperspectral microscope system, where the starting point ($z = 0$ @ the metalens surface) is found by focusing the objective onto the metalens so that surface features of the device are most clearly visible; the transmitted beam is subsequently captured by the microscope camera as the metalens is moved away from the starting position. Both the on-axis and off-axis focusing lenses are designed with an aperture diameter of 2 mm , a focal length of 7 mm , and at the wavelength of $6 \mu\text{m}$.

As shown by the 3-dimensional intensity profile of Fig. 2(a), the beam focuses at about $z = 7.05 \text{ mm}$ after light transmits through the on-axis focusing metalens. 2-dimensional beam profile at the measured focal point is plotted in Fig. 2(b) and a well-defined focal spot is observed. In Fig. 2(d), the measured 1-dimensional intensity curve (x -cut data at $y = 0$ and $z = 7.05 \text{ mm}$) is shown to match with the diffraction limited Airy function. As a result, the focal spot is measured to have a beam size of $32 \mu\text{m}$. An SEM image showing the full top view of the on-axis focusing metalens

is presented in the inset of Fig. 2(c). The metalens is axisymmetric and the resultant focal spot is at the center of the lens.

In contrast, structural profile of the off-axis focusing lens is not axisymmetric. As shown by the SEM image of the off-axis metalens in Fig. 2(b), the center of the meta-structure fringes is located on the right edge of the lens. Both the 3-D intensity profile of Fig. 3(a) and the beam center shift of Fig. 3(b) show clearly that light is focused obliquely as it propagates after the off-axis focusing metalens. Figure 3(b) further reveals that the off-axis angle can be estimated by tracing the beam shift in +x (where the focused beam is deflected) with respect to the z-distance. The angle is calculated as 9.7° , which is close to the designed value (10°). According to the data of Fig. 3(a), the focal length of the off-axis lens is found to be 7.1 mm. Figure 3(c) shows the 2-dimensional beam profile at the measured focal spot, while Fig. 3(d) plots the 1-D intensity distribution of the focal spot alongside the Airy function. The measured data at the focal spot agrees well with the diffraction-limited Airy disk and the focal beam size is found to be $29.6 \mu\text{m}$.

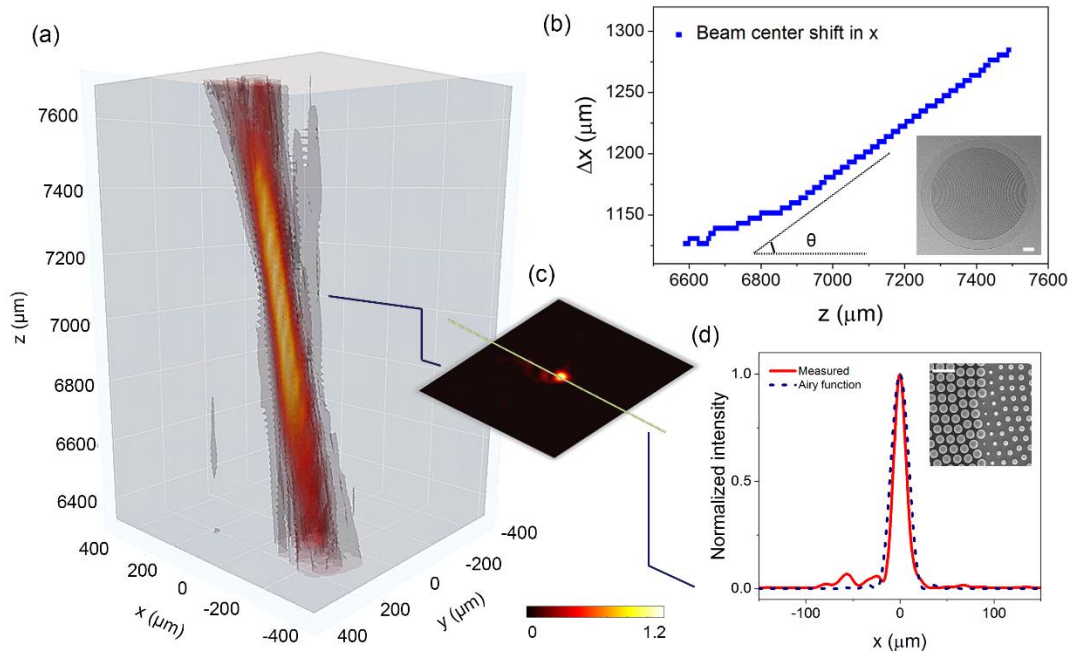


Fig. 3 Measurement data for the off-axis focusing metalens: (a) 3-D intensity profile around the focal point; (b) beam center shift in x-axis against distance to the metalens, inset: SEM image of the full off-axis focusing metalens (scale bar = $200 \mu\text{m}$); (c) xy intensity profile at $z = 7.1 \text{ mm}$; (d) x-cut intensity plot of (c) at $y = 0$ with the Airy function drawn as reference, inset: SEM images of part of the off-axis focusing metalens (scale bar = $4 \mu\text{m}$).

3. Conclusion

In summary, metalenses working at $6 \mu\text{m}$ for on-axis and off-axis focusing are realized on 8-inch Ge-on-Si wafer using CMOS-compatible technology. The measurement results agree well with the design. In the future, we will implement backside polishing and anti-reflection coating for optimum transmission efficiency. The demonstrated mass-producible metasurfaces can be the potential solution for next-generation mid-IR photonics.

This work is supported by Agency for Science, Technology and Research IAF-PP A19B3a0008 and grant C220415015.

4. References

1. S. Zhang, M. Kim, F. Aieta, A. She, T. Mansuripur, I. Gabay, M. Khorasannejad, D. Rousso, X. Wang, M. Troccoli, N. Yu and F. Capasso, "High efficiency near diffraction-limited mid-infrared flat lenses based on metasurface reflectarrays," *Opt. Express*. 24, pp. 18024-18034 (2016).
2. A. Tittl, A.U. Michel, M. Schaferling, X. Yin, B. Gholipour, L. Cui, M. Wuttig, T. Taubner, F. Neubrech and H. Giessen, "A switchable mid-infrared plasmonic perfect absorber with multispectral thermal imaging capability," *Adv. Mater.* 27, pp. 4597-4603 (2015).
3. L. Zhang, J. Ding, H. Zheng, S. An, H. Lin, B. Zheng, Q. Du, G. Yin, J. Michon, Y. Zhang, Z. Fang, M. Y. Shalaginov, L. Deng, T. Gu, H. Zhang and J. Hu, "Ultra-thin high-efficiency mid-infrared transmissive Huygens meta-optics," *Nat. Commun.* 1481 (2018).
4. A. Leitis, M.L. Tseng, A. John-Herpin, Y. S. Kivshar and H. Altug, "Wafer-scale functional metasurfaces for mid-infrared photonics and biosensing," *Adv. Mater.* 33, 2102232 (2021).
5. Y. Zhou, T. Hu, N. Li, Y. Dong, D. Li, Y. H. Fu, Q. Zhong, Z. Xu, S. Zhu, Q. Lin, N. Singh, "A performance study of dielectric metalens with process-induced defects," *IEEE Photonics J.* 12, 4500414 (2020).